

ULRR

The Effect of groundwater level on forced convection heat transfer from a buried cylinder

Item Type	Article
Authors	Oi, Tsubasa;Kimura, Shigeo;Utanohara, Yoichi;Vynnycky, Michael
Citation	Transport in Porous Media
Publisher	Springer
Download date	2025-10-01 18:23:03
Item License	https://creativecommons.org/licenses/by-nc-sa/4.0/
Link to Item	https://doi.org/10.34961/researchrepository-ul.23540289



The Effect of Groundwater Level on Forced Convection Heat Transfer from a Buried Cylinder

Tsubasa Oi^{1,4} · Shigeo Kimura² · Yoichi Utanohara² · Michael Vynnycky³

Received: 5 December 2022 / Accepted: 16 May 2023
© The Author(s) 2023

Abstract

The effect of groundwater level on forced convection heat transfer from a cylinder of 1 m in diameter buried at a depth of 10 m is studied numerically. The porosity and permeability of the soil are fixed at 0.5 and $1.0 \times 10^{-11} \text{ m}^2$, respectively, throughout the present study, while the inlet velocity U_0 and the position of the phreatic surface (h), measured from the center of the cylinder, are varied in the ranges from 10^{-9} to 10^{-3} m s^{-1} and from -4 to 4 m , respectively. Under these conditions, the heat fluxes on the cylinder are computed numerically. Various approximate solutions are also proposed and compared with those obtained numerically. The heat transfer results are also presented in nondimensional form for generality. The paper is divided into three parts, depending on the relative positions of the phreatic surface to the heated cylinder. First, the heat transfer rates are analyzed when the phreatic surface is above the cylinder, so that the cylinder is completely submerged in the water. In the second case, the phreatic surface is assumed to lie below the cylinder, so that the cylinder is left in the water-free space. In the third case, the phreatic surface is in contact with the cylinder surface, so that the cylinder is partially submerged in groundwater. For the above respective cases, three different approximate analyses are presented, and their validities and limitations are evaluated in comparison with the numerical calculations.

Keywords Porous media · Heat transfer · Forced convection · Partially submerged · Heated cylinder · Groundwater

List of symbols

c_p	Specific heat at constant pressure ($\text{J kg}^{-1} \text{K}^{-1}$)
d	Diameter of circular cylinder (m)
d_p	Mean diameter of grains forming porous matrix (m)
Da	Darcy number, $K d^{-2}$ (-)

✉ Michael Vynnycky
michael.vynnycky@ul.ie

¹ Graduate School of Natural Science and Technology, Kanazawa University, Kakuma-machi, Kanazawa 920-1192, Japan

² Faculty of Production Systems Engineering and Sciences, Komatsu University, Shichou-machi, Komatsu, Ishikawa 923-8511, Japan

³ Department of Mathematics and Statistics, University of Limerick, Limerick V94 T9PX, Ireland

⁴ Present Address: Denso, Showa-machi 1-1, Kariya, Aichi 448-8661, Japan

\mathbf{g}	Gravitational acceleration vector (m s^{-2})
h	Position of phreatic surface measured from the center of the cylinder (m)
\bar{h}	Average heat transfer coefficient ($\text{W m}^{-2} \text{K}^{-1}$)
k	Thermal conductivity ($\text{W m}^{-1} \text{K}^{-1}$)
K	Permeability of porous medium (m^2)
Nu	Local Nusselt number: $q''d/((T_h - T_0)k_{\text{eff}})$ (–)
$\bar{\text{Nu}}$	Average Nusselt number: $\bar{q}''d/((T_h - T_0)k_{\text{eff}})$ (–)
P	Dynamic pressure (N m^{-2})
Pe	Péclet number U_0d/α (–)
q''	Local heat flux on the cylinder (W m^{-2})
\bar{q}''	Average heat flux on the cylinder (W m^{-2})
\mathbf{q}	Heat flux vector (W m^{-2})
s	Arc length of circular cylinder (m)
T	Temperature (K)
u	x -Component of \mathbf{u} (m s^{-1})
v	y -Component of \mathbf{u} (m s^{-1})
\mathbf{u}	Groundwater velocity vector (m s^{-1})
U_0	Incoming groundwater velocity (m s^{-1})

Greek Letters

α	Thermal diffusivity of porous medium: $k_{\text{eff}}/(\rho c_p)_f$ ($\text{m}^2 \text{s}^{-1}$)
ε	Porosity of porous medium (–)
μ	Viscosity of groundwater (Pa s)
ρ	Density (kg m^{-3})
ψ	Ratio of wetted arc to the circumference of circular cylinder (–)

Subscripts

air	Saturated with air
eff	Effective physical value
f	Saturating fluid
h	Cylinder temperature
s	Porous matrix
w	Boundary wall
0	Incoming groundwater
∞	Referring to $h = 10$ m

1 Introduction

Flow in porous media is a very important research subject because of its wide-ranging applications, such as geophysical processes to advanced technologies, e.g., fuel cell development as reported by Rosli et al. (2009). In geophysics, the dynamics of fluid flows in porous media was first studied in connection with groundwater hydrology, as summarized by such authors as Bear (1979) and Hillel (1982). Geothermal energy development is another closely related example, where the idea of transport in porous media plays an important role. The geothermal energy is stored in the deep underground permeable layer, called geothermal reservoir, in the form of hot brine, and it must be tapped to the Earth's surface for electricity generation. The geothermal reservoir's dynamical behavior necessary for sustainable steam production

is often analyzed with a model of saturated porous medium. Early development of geothermal energy and its conversion to electricity was well documented by Di Pippo (1980). More recent information on this subject is also available in Di Pippo (2015). Early work on heat transfer and convection in geothermal reservoirs was conducted by Cheng (1978), and Garg and Kassoy (1981). Recent understanding on deep underground reservoirs, however, is that they are more properly modeled as a fracture network system rather than a porous medium, as demonstrated by Zimmerman and Bodvarsson (1996), and more recently Aghajannezhad et al. (2021). Because of high temperature in the reservoir, steam-liquid two-phase convection is possible, as shown by Schubert and Straus (1977, 1979), and a recent review on this subject is available in Valavanides (2018). Low-enthalpy geothermal energy can be also tapped with ground-coupled heat pumps (GCHP). This direct use of thermal energy for building heating and agricultural greenhouses is a fast-growing industry today, as reviewed by Sarbu and Sebarchievici (2016), and amply documented in the handbook from ASHRAE (American Society of Heating and Air-Conditioning Engineers) (2021).

Heat transfer from a heated object placed in the ground is often encountered in both high- and low-enthalpy geothermal energy developments. For example, Cheng and Minkowycz (1977) investigated natural convection from a hot intrusion in a geothermal system. Merkin (1979) studied natural convection from a general two-dimensional heated body. Since then, there have appeared numerous research reports on natural convection around heated bodies in porous media with various different flow models, such as: non-Darcy flow models; non-Newtonian fluid-filled porous media; non-uniform permeability distributions; conduction and convection conjugate problems. The aforementioned problems are compiled in reference books such as those by Bejan and Kraus (2003), Nield and Bejan (2013) and Vafai (2015).

Although it is less prevalent, forced convection heat transfer from a heated circular cylinder embedded in a porous medium is an important subject in connection with borehole heat exchangers (BHE) employed in GCHP, as described by Ngo and Lai (2009). Groundwater flow influence on BHE performance was examined by such authors as Diao et al. (2004), Katsura et al. (2006), Lee and Lam (2007), Wang et al. (2009), Holmberg et al. (2016), Li et al. (2020) and Casasso and Sethi (2014). According to these authors, the presence of groundwater flow noticeably enhances BHE performance. In order to understand the mechanism of this enhancement, forced convection heat transfer from an isothermal cylinder may serve as a basis for the analysis.

Early work on forced convection heat transfer from a heated cylinder dates back to Cheng (1982), who employed the Darcy model for fluid flow through a porous matrix and the local thermal equilibrium condition between the porous matrix and saturated fluid. However, he did not report the average heat transfer coefficients, which are often more important from the engineering point of view. Integrating the local values of heat flux over the cylinder surface, the average heat transfer coefficients were presented in the book by Nield and Bejan (2013). Forced convection heat transfer from a heated elliptic cylinder was analyzed by Kimura (1988a), which plays a role to bridge heat transfer from a flat plate and that from a circular cylinder. Kimura (1989) also considered transient heat transfer from an isothermal circular cylinder. When a constant flux is specified over a circular cylinder, Kimura (1988b) carried out a boundary-layer analysis and devised groundwater velocimetry. A groundwater velocimeter based on this idea was constructed and reported by Kimura (2015).

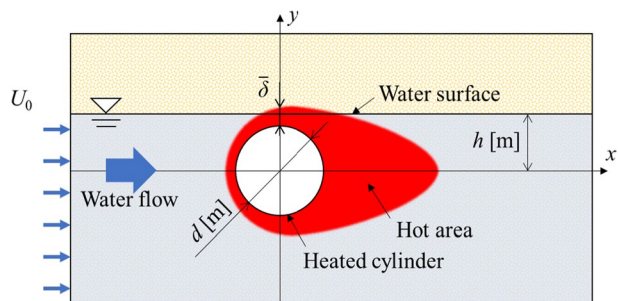
Experimental work on the heat transfer in a packed bed was performed by Nasr et al. (1994). Their main interest was the enhancement of heat transfer from an isothermal cylinder by high-conductivity packed-bed materials. The validity of the above-mentioned averaged heat transfer characteristics was marginally verified in their experiments. The forced

convection in a packed bed is mainly focused on a high fluid velocity regime. Therefore, it is natural that the research has been directed toward heat transfer analyses using various non-Darcy flow models, and the eventual relaxation of the local thermal equilibrium (LTE) condition between the fluid and the porous matrix. These non-Darcy flow models and local thermally non-equilibrium (LTNE) models require the introduction of new parameters. Therefore, the mathematical system that describes the conservation laws becomes increasingly more complex, and we are still far from a complete understanding of heat transfer behavior in those models. Nonetheless, research reports on packed beds have been published by many authors. For example, heat transfer from an isothermal cylinder based on various extended Darcy models was reported on by such authors as Thevenin and Sad-aoui (1995) and Layeghi and Nouri-Borujerdi (2004). It is expected that the LTE condition between the fluid and solid phases will become less valid as the heat transport speeds in the fluid and solid become significantly different, which is conceivable when the flow speed increases. This local thermally non-equilibrium problem was investigated with the Darcy flow model by Rees et al. (2003) and Wong et al. (2004). Al-Sumaily et al. (2012) presented a numerical analysis with the Brinkman-extended non-Darcy flow model and LTNE condition.

The above brief review on forced convection from a heated circular cylinder reveals the basic assumption common to all: the porous medium is completely saturated with flowing fluid. On the other hand, McKibbin and Kimura (2014) were the first to propose a problem in which the heated cylinder was partially submerged in groundwater, i.e., the cylinder was positioned near the interface between a water-saturated lower layer and an air-saturated upper layer, as shown in Fig. 1. The problem was inspired by the need to evaluate the heat transfer from a buried circular tank filled with water, which can serve as a possible heat reservoir for heat pump systems in the heating and cooling of residential or office buildings. In such a case, the tank is frequently either fully or partially submerged in the groundwater. In order to define the heat transfer problem from the water-filled tank, it is necessary to introduce two additional parameters: the relative positions of the groundwater level and ground surface to the buried cylinder. This makes the proposed problem rather intractable. Although the paper demonstrated the mathematical power to compute the heat transfer for several sets of the above two geometric parameters, it suffers from the lack of a general picture of heat transfer characteristics as the parameters involved are varied.

In the present paper, we relax one of the geometric conditions, i.e., the relative position of the ground surface to the tank, which means that the tank is positioned far from the ground surface. This simplification makes the problem much more tractable. Therefore, the present paper is only concerned with the groundwater level relative to the tank. We further model the tank as an isothermally heated circular cylinder in the two-dimensional plane.

Fig. 1 Schematic diagram of the numerical model for the heated cylinder buried in a saturated porous medium with a phreatic surface



The present paper is divided into the following three parts: (a) the cylinder is completely submerged in shallow groundwater; (b) the cylinder is positioned above the groundwater surface, also called the phreatic surface, but only by a small distance; (c) the cylinder is partially submerged in groundwater. We show in this paper a general picture of heat transfer characteristics for the respective categories. Case (a) is illustrated schematically in Fig. 1.

We start with the mathematical formulation and the definition of the domain to be analyzed, along with the boundary conditions. Then, we conduct numerical computations to generate heat transfer results for a given set of parameters in the respective cases. We also provide simple analyses to delineate physical reasons for the observed heat transfer characteristics. Lastly, the conclusions of the present work are drawn.

2 Mathematical Formulation

2.1 The Governing Equations

In this section, we describe a mathematical system derived from the mass, momentum and energy conservation laws in a saturated porous medium. We are concerned with the heat transfer in the ground, where the groundwater velocity is usually small, typically 0.001 to 1 mm s⁻¹ in Darcy velocity, and the average particle size composing the porous matrix is typically less than 1 mm. The permeability is usually of the order of 10⁻¹¹ m². Due to the above conditions, it is generally believed that the Darcy law and the LTE condition are guaranteed. The conservation equations for mass, momentum and energy in vectorial form are:

$$\nabla \cdot \mathbf{u} = 0, \tag{1}$$

$$\frac{1}{\varepsilon^2} \rho(\mathbf{u} \cdot \nabla)\mathbf{u} = \nabla \cdot \left[-p\mathbf{I} + \frac{\mu}{\varepsilon} (\nabla\mathbf{u} + (\nabla\mathbf{u})^T) \right] - \frac{\mu}{K\varepsilon} \mathbf{u} + \rho\mathbf{g}, \tag{2}$$

$$\rho c_p \mathbf{u} \cdot \nabla T + \nabla \cdot \mathbf{q} = 0, \mathbf{q} = -k_{\text{eff}} \nabla T. \tag{3}$$

Here, we employ the Brinkman-extended momentum equation. In the above equations, \mathbf{u} is a velocity vector, \mathbf{g} is the vector of gravitational acceleration, \mathbf{I} is the identity matrix, and P is the dynamic pressure. ρ , μ and c_p are the fluid density, viscosity and specific heat, respectively. The effective thermal conductivity of the porous medium is defined as $k_{\text{eff}} = k_f \varepsilon + k_s (1 - \varepsilon)$, where the subscripts s and f indicate the porous matrix and the saturating fluid, respectively, with ε as the porosity and K as the permeability.

2.2 The Physical Properties and Parameters Employed in the Present Paper

The physical properties of air and water at $T_0 = 293.15$ K (inlet water temperature) are used for the present numerical computations. The cylinder temperature is fixed at $T_h = 303.15$ K. The physical properties of the porous matrix are taken from the data generally accepted in groundwater hydrology, e.g., Bear (1979), and they are listed in Table 1. In a typical sand and gravel layer in an aquifer, it is known that the porosity varies from 0.4 to 0.5, and the mean grain size is between 0.1 and 1 mm. The permeability is in the order of 10⁻¹¹ m². It is worth noting that the Carman–Kozeny formula, $K = d_p^2 \varepsilon^3 / (180(1 - \varepsilon)^2)$, for

Table 1 Physical properties of porous matrix

Thermal conductivity k_s ($\text{W m}^{-1} \text{K}^{-1}$)	2.45
Density ρ_s (kg m^{-3})	2643
Specific heat c_{ps} ($\text{J kg}^{-1} \text{K}^{-1}$)	710

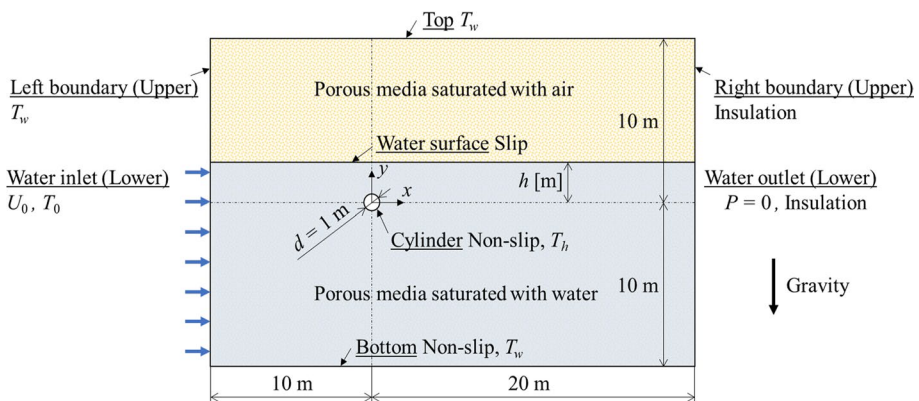
example, see Nield and Bejan (2013), gives $2.78 \times 10^{-11} \text{ m}^2$ for spherical beads for which $d_p = 0.1 \text{ mm}$, and the porosity of $\epsilon = 0.5$. Assuming a typical permeable aquifer, the parameters involved in the present work are summarized in Table 2.

2.3 The Computational Domain and the Boundary Conditions

The groundwater level is always positioned close to the cylinder. As shown in Fig. 2, the domain of analysis is $20 \text{ m} \times 30 \text{ m}$, and the center of the circular cylinder (1 m in diameter) is positioned at the mid-height and 10 m from the left boundary. The thermal boundary conditions on the top, bottom and left boundaries are fixed at a constant temperature, and the right boundary is adiabatic. The groundwater enters into the lower layer of the domain through the left boundary at a specified velocity, while the top (phreatic surface) of the water-saturated layer is stress-free and the bottom is non-slip. The right boundary is set to the usual outlet condition with a constant dynamic pressure. The groundwater surface is horizontal, and the capillary fringe is ignored; on the

Table 2 Fixed parameters used in the present study

Ground surface position	10 m above the cylinder
Porosity	$\epsilon = 0.5$ (-)
Permeability	$K = 1.0 \times 10^{-11} (\text{m}^2)$
Cylinder diameter	$d = 1.0 (\text{m})$
Darcy number	$Da = 1.0 \times 10^{-11} (-)$
Initial temperature of porous medium	293.15 (K)
Temperature of incoming groundwater	293.15 (K)
Temperature of cylinder	303.15 (K)

**Fig. 2** Computational domain and the boundary conditions

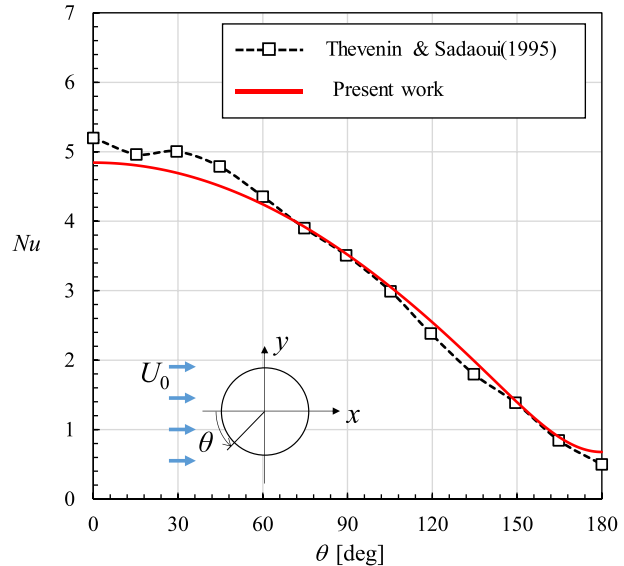
other hand, the upper layer is saturated with dry air, which is assumed to be completely stagnant, and the velocity vector there is set to zero in the momentum and energy equations. Because of the local thermal equilibrium assumption, we solve a single energy equation, with two different fluid properties, i.e., the lower layer has the thermal properties of a water–sand mixture, while the upper layer has the properties of an air–sand mixture. Therefore, the air-saturated upper layer is essentially modeled as a rectangular solid region. Referring to Fig. 2, the domain of analysis and the associated boundary conditions are mathematically expressed as:

$$\begin{aligned}
 &\text{Vertical left } x = -10 \text{ m,} \\
 &T = T_w, u = v = 0 \quad h \leq y \leq 10 \text{ m} \\
 &T = T_0, u = U_0, v = 0 \quad -10 \text{ m} \leq y \leq h \\
 \\
 &\text{Vertical right } x = 20 \text{ m} \\
 &\frac{\partial T}{\partial x} = 0, u = v = 0 \quad h \leq y \leq 10 \text{ m} \\
 &\frac{\partial T}{\partial x} = 0, P = 0 \quad -10 \text{ m} \leq y \leq h \\
 \\
 &\text{Horizontal bottom } y = -10 \text{ m} \quad -10 \text{ m} \leq x \leq 20 \text{ m} \\
 &T = T_w, u = v = 0 \\
 \\
 &\text{Groundwater surface } y = h \quad -10 \text{ m} \leq x \leq 20 \text{ m} \\
 &k_{\text{eff}} \frac{\partial T}{\partial y} \Big|_{y=h-0} = k_{\text{eff,air}} \frac{\partial T}{\partial y} \Big|_{y=h+0}, \quad T_{y=h-0} = T_{y=h+0}, \quad \frac{\partial u}{\partial y} = v = 0 \\
 \\
 &\text{Horizontal top } y = 10 \text{ m} \quad -10 \text{ m} \leq x \leq 20 \text{ m} \\
 &T = T_w, u = v = 0
 \end{aligned} \tag{4}$$

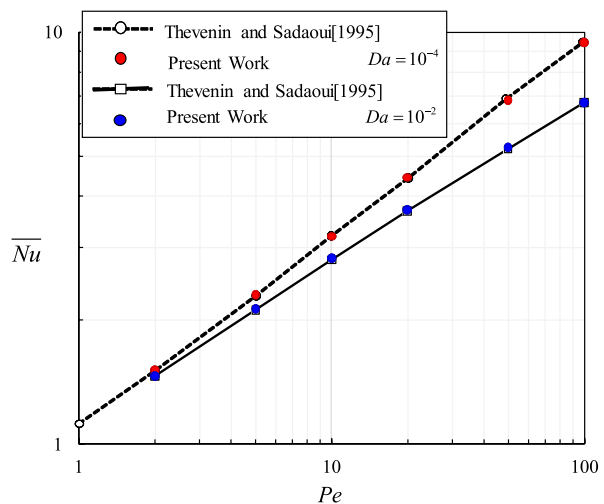
2.4 Numerical Methodology and Validation

The set of the governing Eqs. (1)–(3) were solved together with the above boundary conditions. The COMSOL Multiphysics software Ver.5.4, a finite-element-based numerical solver, was employed to solve the problem. Non-uniform elements were generated over the region external to the cylinder, with mesh refinement being employed near the surface of the cylinder. The total number of elements was 140,540. The local and average Nusselt numbers were compared with those obtained by Thevenin and Sadaoui (1995) for the Darcy numbers $Da = 10^{-2}, 10^{-4}$, the Péclet numbers $Pe = 1 - 10^3$ and the porosity $\epsilon = 0.9$. The local Nusselt number distribution on the cylinder surface at $Pe = 7.0$ is shown in Fig. 3a. Good agreement is observed. The slight difference that is apparent may be due to the rather coarse grid used by Thevenin and Sadaoui (1995). As regards the average Nusselt numbers, the two results are almost identical, as shown in Fig. 3b. It is also worth noting that for $Da = 10^{-4}$ the average Nusselt numbers are very close to the boundary-layer solution with the Darcy flow model, which reads as $\overline{Nu} = 1.015Pe^{1/2}$ (Nielsen and Bejan 2013).

Fig. 3 The present numerical results for local and average Nusselt numbers compared with those by Thevenin and Sadaoui (1995); **a** local Nusselt numbers at $Pe=7$, **b** average Nusselt numbers as a function of the Péclet number for two different Darcy numbers



(a) Local Nusselt numbers at $Pe=7$



(b) Average Nusselt numbers

3 Results and Discussion

3.1 Completely Submerged Cylinder

3.1.1 Numerical Results

The temperature fields near the cylinder for four different water velocities are shown in Fig. 4. In these cases, the cylinder is completely submerged, and the phreatic surface is

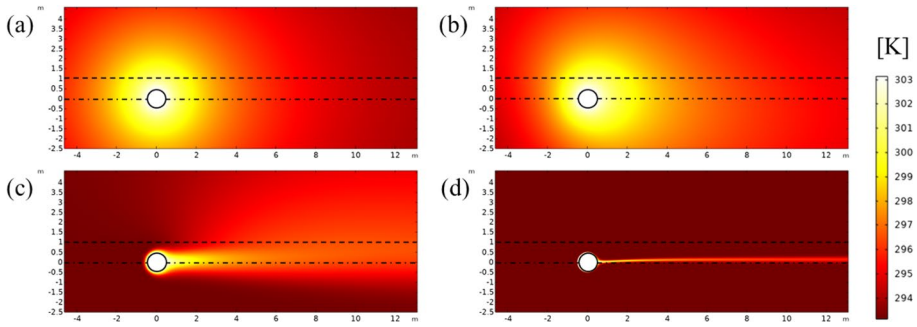


Fig. 4 Temperature distributions around a heated cylinder buried in a porous medium for $h=1$ m with four inlet velocities: **a** $U_0=10^{-9}$ m s $^{-1}$, **b** $U_0=10^{-7}$ m s $^{-1}$, **c** $U_0=10^{-5}$ m s $^{-1}$ and **d** $U_0=10^{-3}$ m s $^{-1}$. Each dashed line represents a water surface. Each dashed-dotted line corresponds to a horizontal line through the center of the cylinder

positioned at 1.0 m from the cylinder center. In the figure, the vertical position of the cylinder center is shown with a dashed-dotted line, and the phreatic surface is indicated with a dashed line. When the water velocity is less than $U_0 = 10^{-7}$ m s $^{-1}$, it is evident that the flow effects are not very visible, and that the heat transfer is dominated by conduction. On the other hand, when the velocity exceeds $U_0 = 10^{-5}$ m s $^{-1}$, a thin thermal boundary along the cylinder is clearly visible. It should be also noted that only the temperature in the water-saturated zone is strongly influenced by the heated cylinder. This situation is further pronounced at $U_0 = 10^{-3}$ m s $^{-1}$. The average Nusselt numbers for all of the combinations of velocity and phreatic surface position are given in Table 3.

In parallel with the temperature fields, we also show the local heat fluxes over the cylinder in Fig. 5. Figure 5a, b clearly indicates that the heat transfer rates are functions of the phreatic surface levels at small groundwater velocities. On the other hand, Fig. 5c, d, for large groundwater velocities, shows no dependence on the phreatic surface level. This further enforces our previous argument.

3.1.2 Effects of the Phreatic Surface

The series of temperature fields at different groundwater velocities in Fig. 4 prompts us to look in more depth at the relative thickness between the thermal boundary layer and the

Table 3 Average Nusselt numbers computed for five different phreatic surface levels and seven different Péclet numbers

h/d	$Pe/2.74$						
	10^{-3}	10^{-2}	10^{-1}	1	10^1	10^2	10^3
10	0.6312	0.6326	0.7326	1.8256	5.6880	18.0388	56.8664
4	0.6179	0.6191	0.7119	1.8241	5.6962	18.0760	56.9936
3	0.6134	0.6146	0.7000	1.8231	5.7040	18.1040	57.0839
2	0.6068	0.6078	0.6820	1.8085	5.7273	18.1826	57.3335
1	0.5951	0.5959	0.6534	1.6541	5.8536	18.6071	58.6686

The Péclet numbers were divided by 2.74 in order to avoid fractional values

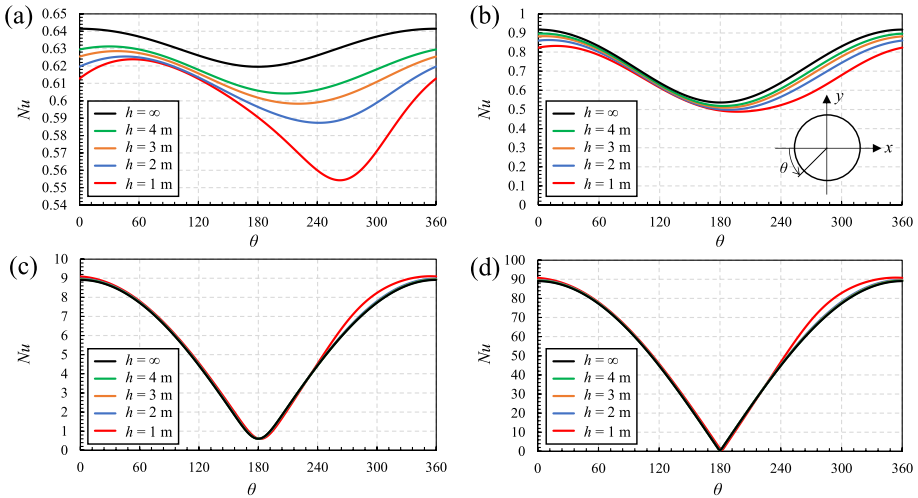


Fig. 5 Local Nusselt numbers over a heated cylinder buried in a porous medium for $h=1$ m with four different inlet velocities: **a** $U_0=10^{-9}$ m s $^{-1}$, **b** $U_0=10^{-7}$ m s $^{-1}$, **c** $U_0=10^{-5}$ m s $^{-1}$ and **d** $U_0=10^{-3}$ m s $^{-1}$

submerged depth. When the submerged depth is given as a condition, there is a critical velocity, beyond which the thermal boundary layer is confined to the water-saturated zone, and consequently the presence of the phreatic surface does not influence the heat transfer rate over the cylinder. In this case, the heat transfer can be obtained in the same way as a case in which the region is completely saturated with groundwater.

Here, we try to determine the critical velocity when the depth of the submerged cylinder is given. Since this is only a rough argument, we are only concerned with the average value of the boundary-layer thickness. According to the boundary-layer theory, the average thickness over the cylinder is inversely proportional to the square root of the Péclet number (Nield and Bejan 2013). Therefore, when the depth is equal to the thermal boundary-layer thickness $\bar{\delta}$, the corresponding velocity, which is expressed as a function of the Péclet number, is the critical velocity; in this case,

$$h - \frac{d}{2} = \bar{\delta} = a \cdot dPe^{-0.5}, \tag{5}$$

where a is an arbitrary $O(1)$ constant. The value of a will be determined by comparing the average Nusselt number \overline{Nu}_∞ with $h=10$ m and the numerical results for \overline{Nu} with an arbitrary submerged depth. We compute the relative differences of the two defined by Eq. (6) and show them in Fig. 6:

$$\Delta \overline{Nu} = \left| \frac{\overline{Nu}}{\overline{Nu}_\infty} - 1 \right| \times 100\% \tag{6}$$

In the figure, it should be noted that the Péclet number appearing in the abscissa is divided by 2.74 in order to avoid fractional numbers in the abscissa scales. In this way, we can easily relate the value of the Peclet number with the actual incoming water velocity, i.e., $Pe/2.74=1$ corresponds to $U_0 = 10^{-6}$ m s $^{-1}$. It seems that $a = 2$ in Eq. (5) fits well in

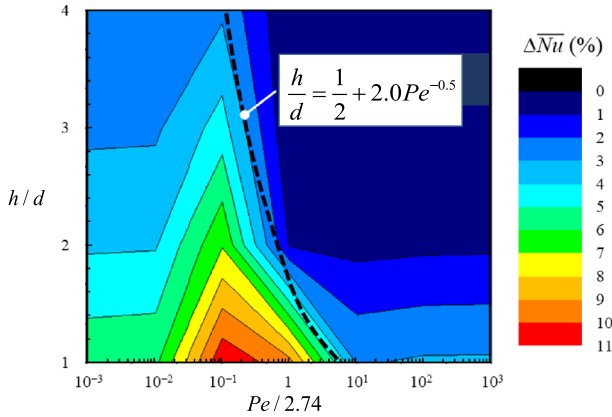


Fig. 6 Contours of the percentage differences of the average Nusselt numbers compared with fully submerged cases with $h = 10$ m. The broken line represents the boundary line of Eq. (5), proposed in the present theoretical model with $a = 2$. The Péclet numbers were divided by 2.74 so that the abscissa scales are round numbers. Note that the present numerical simulations were all carried out with dimensional numbers. The dimensional groundwater velocities are obtainable by multiplying abscissa scales with 10^{-6} m s^{-1}

order to divide the range into small and large $\Delta \overline{Nu}$ regions. For example, when the submerged depth is equal to the radius of the cylinder, i.e., $h/d = 1$ in Fig. 1, the heat transfer can be estimated by the boundary-layer theory as long as the Péclet number is greater than 16.

3.2 Cylinder Positioned Above the Phreatic Line

3.2.1 Numerical Results

The numerical computations are performed when the phreatic surface is positioned below the cylinder. In this case, h takes a negative value and it must satisfy the condition $h < -d/2$. In Fig. 7, the temperature fields are shown for two different groundwater velocities, $U_0 = 10^{-6} \text{ m s}^{-1}$ and 10^{-3} m s^{-1} , when the phreatic surface is set to $h = -1$ m, where the dashed-dotted and dashed lines indicate the cylinder center and the phreatic surface, respectively, as before. When the velocity is $U_0 = 10^{-6} \text{ m s}^{-1}$, a temperature rise near the cylinder can be observed both in the water- and the air-saturated layers. On the other hand, no temperature rise is observed in the water-saturated layer when the velocity is 10^{-3} m s^{-1} . This is because the flowing groundwater quickly sweeps away the conducting heat from above, when the velocity is large. Therefore, the phreatic surface is kept at a nearly constant temperature equal to the incoming water temperature.

3.2.2 Approximate Evaluation of Heat Transfer Rate Due to Mirror-Image Method

The above observation of the temperature fields suggests the possibility of obtaining an analytical solution for large groundwater velocities. In that case, the phreatic surface can be assumed to be at a constant temperature equal to that of the incoming water. This is the problem of heat conduction in a semi-infinite space, where a constant temperature cylinder

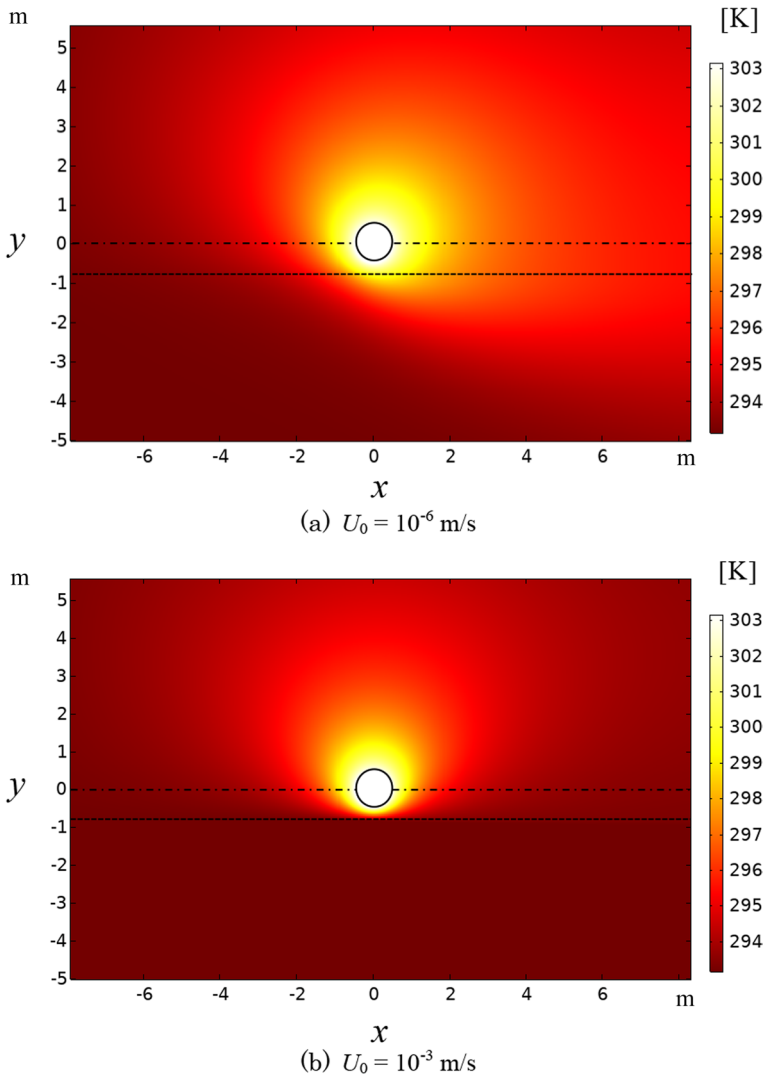


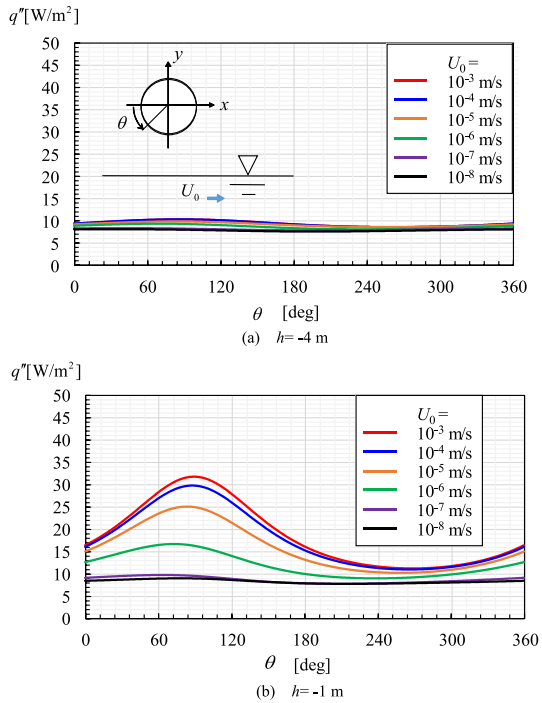
Fig. 7 Temperature fields of the numerical solution when the phreatic surface is $h = -1$ m and two different groundwater velocities: **a** $U_0 = 10^{-6}$ m s $^{-1}$; **b** $U_0 = 10^{-3}$ m s $^{-1}$

is placed above the reflection boundary at a different constant temperature. The problem can be solved with the mirror-image method, as described in the book by Eckert and Drake (1972). The average heat flux over the cylinder is given in nondimensional form by

$$\frac{\bar{q}'' d}{k_{\text{eff,air}}(T_h - T_0)} = \frac{1}{\ln \left[2(|h|/d) + \sqrt{4(h/d)^2 - 1} \right]}. \quad (7)$$

In Fig. 8, we show local heat flux variations obtained by numerical computations. When $h = -4$ m, the heat fluxes are nearly independent of the groundwater velocity.

Fig. 8 Local heat fluxes for six different groundwater velocities with two different phreatic levels: **a** $h = -4$ m, **b** $h = -1$ m



This is understandable, because the magnitude of the temperature gradient becomes smaller as one moves away from the heated object. Therefore, the thermal property there is less influential on the heat flux over the cylinder. On the other hand, when $h = -1$ m, the groundwater velocity greatly influences heat transfer rates over the cylinder. In this case, contrary to the former example, the temperatures very close to the cylinder are significantly altered by the presence of groundwater. The heat flux becomes large as the velocity becomes large. This is because the nearly constant temperature on the phreatic surface at a large velocity forms a steep temperature gradient under the cylinder.

In Fig. 9, we plot the average heat flux as a function of the position of the phreatic surface, in both dimensional and nondimensional forms. The dashed line is obtained by using Eq. (7), whereas the other lines are obtained numerically for the different velocities and phreatic surface levels. It is clearly seen that Eq. (7) and the numerical computations give nearly identical results when the water velocity is greater than $U_0 = 10^{-4}$ m s⁻¹. At $U_0 = 10^{-5}$ m s⁻¹, the values predicted by Eq. (7) are still useful if errors of about 20% are accepted. However, at $U_0 = 10^{-6}$ m s⁻¹, the numerical solutions start deviating greatly from those given by Eq. (7). As the groundwater velocity decreases, the position of the phreatic surface becomes less influential on the resulting heat transfer. This, as discussed before, is due to the fact that the heat transfer is essentially determined by the temperature gradient in the region close to the cylinder, and the far-field temperatures become less significant. It is also instructive to compute the conductive heat flux on an isothermal cylinder placed in an air-saturated porous medium with the physical properties in Table 1 and the same temperature difference at a very large time. According to Carslaw and Jaeger (1946), the average heat flux on the

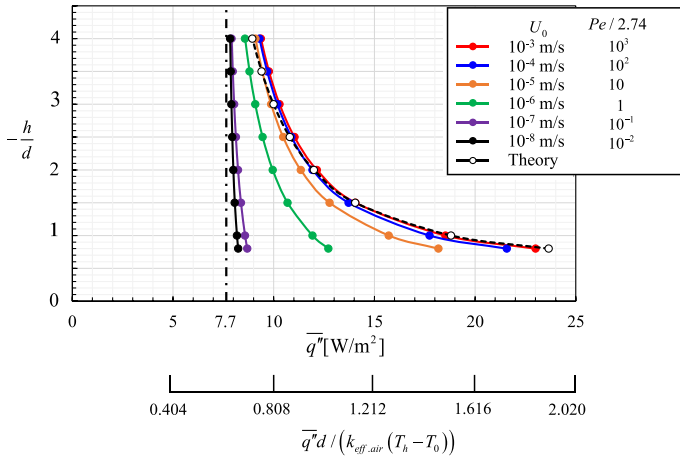


Fig. 9 The average heat fluxes predicted by the mirror-image method compared with the numerical results for six different groundwater velocities and eight different positions of the phreatic surface. The vertical dashed-dotted line for $\bar{q}'' = 7.7 \text{ W m}^{-2}$ is shown as a reference value of the heat flux when the cylinder is placed in an infinite air-saturated porous layer and the elapsed time is about 280 days. In the legend, the Péclet numbers were divided by 2.74 for the same reason as in Fig. 6

cylinder surface is about $7.7 \text{ (W m}^{-2}\text{)}$ at 280 days elapsed time, and this value continues to decrease indefinitely as time passes.

3.3 Partially Submerged Cylinder

3.3.1 Numerical Results

The third case is a situation in which the cylinder is partially submerged in the groundwater. In the present paper, this is equivalent to saying that the parameter h is in the range $-0.5 \text{ m} < h < 0.5 \text{ m}$. In Fig. 10, the temperature fields near the cylinder for $U_0 = 1.0 \times 10^{-3} \text{ (m s}^{-1}\text{)}$ for three different positions of phreatic surface level are shown. A large rise in temperature in the dry upper layer and thin thermal boundary layer in the lower water-saturated zone is common to all three figures. This implies that the thermal resistance over the cylinder facing to the dry upper layer is much greater than that on the portion facing to the water-saturated lower layer. The figures indicate that this is true irrespective of the phreatic surface levels. This point is further demonstrated in Fig. 11, where the local heat fluxes are plotted as a function of the angle θ . In the graphs, the heat fluxes on the portion wetted with groundwater are generally much greater than those on the dry portion. This feature is more pronounced as the groundwater velocity increases. However, even at the velocity of $U_0 = 1.0 \times 10^{-6} \text{ (m s}^{-1}\text{)}$, a substantial difference between the two is still visible.

An additional interesting observation is made when $h < 0$. As seen in Fig. 11c, a spike-like heat flux appears at the circumferential position at which the groundwater first strikes the cylinder. There, the incoming cold groundwater meets the hot cylinder wall with almost no deceleration in the velocity. This situation forms a singularity in the temperature gradient at that position; on the other hand, for $h > 0$, the incoming groundwater must reverse

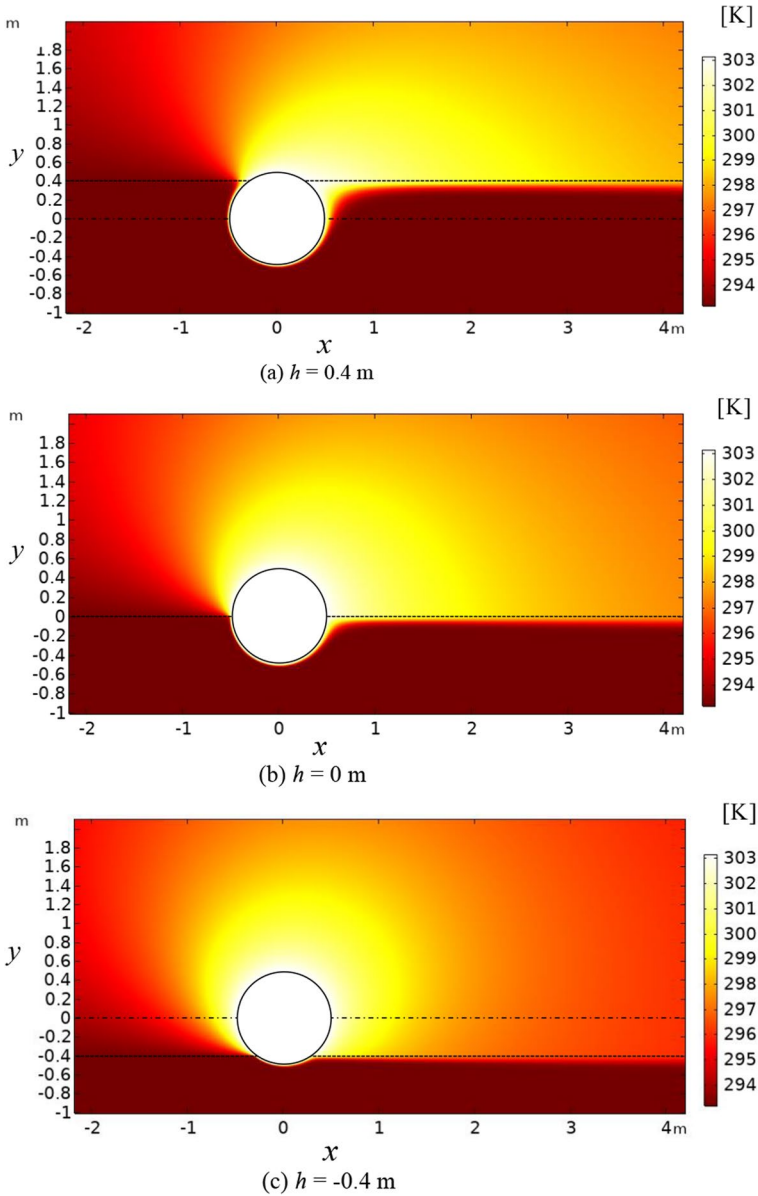


Fig. 10 Temperature fields near the cylinder at three different positions of the phreatic surface with the same groundwater velocity of $U_0 = 10^{-3} \text{ m s}^{-1}$: **a** $h = 0.4$ m; **b** $h = 0$ m; **c** $h = -0.4$ m

or greatly alter its flow direction before striking the cylinder. This creates a nearly stagnant region in front of the cylinder, in which thermal diffusion may be the dominant mechanism. This is the reason why, with $h = 0.4$ m, the heat flux smoothly increases from the position where the phreatic surface meets the cylinder. In the $h = 0$ m case, the flow changes its direction only by 90° degrees, and there is no reversed velocity component. Therefore, the

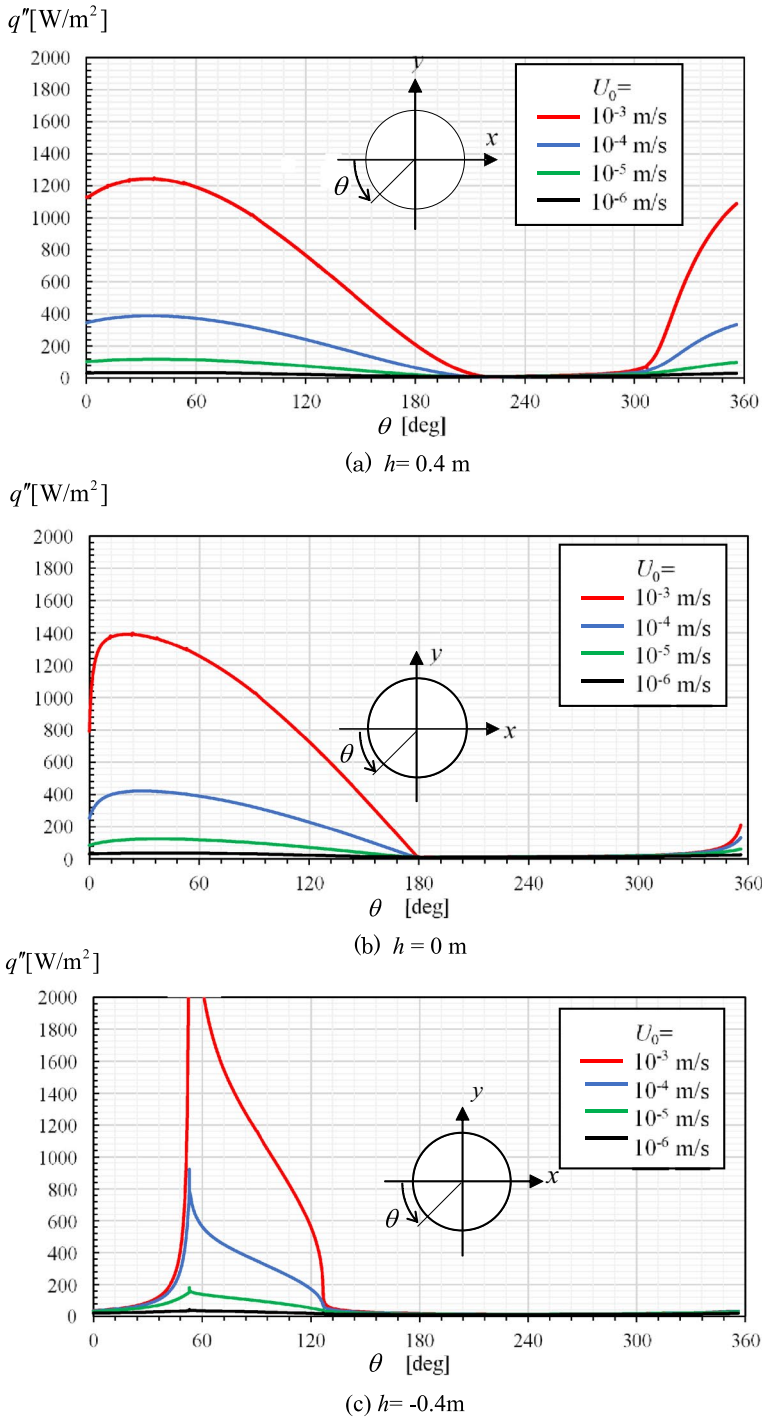


Fig. 11 Local heat fluxes over the heated cylinder for four different groundwater velocities, where the phreatic surface is positioned at three different levels: **a** $h = 0.4 \text{ m}$; **b** $h = 0 \text{ m}$

Table 4 Numerically obtained mean heat fluxes $\overline{q''}$ (W m^{-2}) over the heated cylinder for four different groundwater velocities and nine different positions of the phreatic surface

h (m)	U_0 (m s^{-1})			
	10^{-3}	10^{-4}	10^{-5}	10^{-6}
0.4	562.87	178.39	57.53	20.41
0.3	542.04	172.27	55.92	20.07
0.2	519.55	165.64	54.18	19.72
0.1	495.04	158.42	52.30	19.35
0.0	467.94	150.46	50.25	18.96
- 0.1	437.42	141.54	47.98	18.55
- 0.2	401.98	131.28	45.43	18.11
- 0.3	358.47	118.92	42.48	17.62
- 0.4	299.04	102.66	38.85	17.07

stagnant region is much smaller, and the heat flux starts rising sharply, yet no spike-like heat flux is produced, as seen in Fig. 11b. In summary, the numerically obtained average heat fluxes over the cylinder are listed with various combinations of the groundwater velocity and the phreatic surface level in Table 4.

3.3.2 Rough Estimate of Average Heat Transfer Rate

The above observations prompt us to formulate a method that can approximately evaluate the average heat flux on the cylinder, or the total heat flow from the cylinder. Suppose that we have a given condition for the incoming groundwater velocity, and that the cylinder is completely submerged. If this is the case, the average Nusselt number is given by $\overline{Nu} = 1.015Pe^{1/2}$. If the cylinder is partially submerged, the first approximation is to neglect the heat flow on the cylinder wall contacting with the upper dry layer, compared with the heat flow on the lower wet layer, as seen in Fig. 11. That is to say, the heat flow takes place only on the portion where the cylinder wall is contacting with the water-saturated lower layer. In doing so, we first define the fraction of the arc length, s , over the total peripheral length,

$$\psi = \frac{s}{\pi d}. \tag{8}$$

In order to compute the average heat flux, we simply multiply the average heat flux from the completely submerged case with the fraction ψ defined by Eq. (8), i.e.,

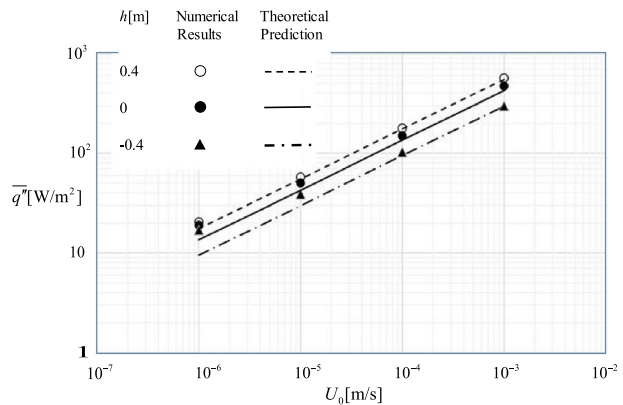
$$\overline{q''} = \overline{h}(T_h - T_0)\psi = 1.015 \frac{k_{\text{eff}}}{d} Pe^{1/2} (T_h - T_0)\psi. \tag{9}$$

The results obtained from Eq. (9) are listed in Table 5. The above results compare well with the numerical ones listed in Table 4, especially when both the groundwater velocity and the wetted fraction are large. This is quite understandable, because the basis of the approximate method is $\overline{Nu} = 1.015Pe^{1/2}$, which is derived from the boundary-layer assumptions. Also, since the heat flow from the portion that is in contact with the dry layer is completely neglected in Eq. (9), the approximation must be more accurate as the fraction ψ is large and close to unity. This translates into that the average heat

Table 5 Mean heat fluxes \overline{q}'' (W m^{-2}) over the heated cylinder, based on Eq. (7), for the same conditions as in Table 4

h (m)	U_0 (m s^{-1})			
	10^{-3}	10^{-4}	10^{-5}	10^{-6}
0.4	547.2	175.5	54.7	17.5
0.3	509.0	163.3	50.9	16.3
0.2	477.8	153.3	47.8	15.3
0.1	449.6	144.2	45.0	14.4
0.0	422.5	135.5	42.3	13.6
-0.1	395.4	126.8	39.5	12.7
-0.2	367.2	117.7	36.7	11.8
-0.3	336.0	107.7	33.6	10.8
-0.4	297.8	95.5	29.8	9.55

Fig. 12 Mean heat fluxes \overline{q}'' (W m^{-2}) over the heated cylinder, as a function of groundwater velocity U_0 (m s^{-1}), with three different locations of the phreatic surface: $h=0.4$ m, 0 m, -0.4 m



flux values in the upper left region of the two tables compare well, whereas those in the lower right region of the two compare rather poorly. Nonetheless, the simplicity of Eq. (9) should be appreciated. The above observations can be summarized graphically in Fig. 12.

4 Concluding Remarks

Forced convection heat transfer from a circular cylinder placed in soil in the presence of the phreatic surface has been investigated. The two-dimensional space subject to analysis is composed of two horizontal layers, where the upper one is saturated with stagnant air, and the lower is saturated with flowing groundwater. The ground surface is fixed 10 m above the cylinder, and the problem is addressed for the three different phreatic surface levels relative to the cylinder: (a) the cylinder is completely submerged in shallow groundwater; (b) the cylinder is positioned above the groundwater surface, but only by a small distance; (c) the cylinder is partially submerged in groundwater. The physical properties of the porous matrix are chosen from those in a typical permeable aquifer.

1. When the heated cylinder is completely submerged, the critical groundwater velocity is determined by Eq. (5), beyond which the average heat transfer can be computed as that in an infinite groundwater-saturated medium.
2. When the heated cylinder is situated above the phreatic surface level, a simple formula to compute the average heat transfer rate is proposed. Its validity has been extensively tested via numerical simulations. It has been proved that the formula in Eq. (7) gives good predictions when the groundwater velocity is such that $Pe > 27.4$.
3. When the heated cylinder is partially submerged, the heat transfer is essentially controlled by the arc length contacting with the water-saturated layer. This observation allows us to introduce the simple formula of Eq. (9), i.e., the heat transfer rate for the completely submerged case multiplied by a wetted arc length ratio to the circular perimeter. Extensive numerical verifications have been conducted, and it is found that the formula gives good predictions, particularly when the groundwater velocity and the wetted arc length ratio are large.

Acknowledgements This work has been done as the thesis study of Mr Tsubasa Oi, for a partial requirement for his Master's Degree. Portions of the present work have been reported a few times in both international and domestic academic meetings.

Funding Open Access funding provided by the IReL Consortium. The work was done using ordinary research budgets provided to faculty members by Komatsu University and Kanazawa University, not via an external award.

Declarations

Conflict of interest The authors have not disclosed any competing interests.

Open Access This article is licensed under a Creative Commons Attribution 4.0 International License, which permits use, sharing, adaptation, distribution and reproduction in any medium or format, as long as you give appropriate credit to the original author(s) and the source, provide a link to the Creative Commons licence, and indicate if changes were made. The images or other third party material in this article are included in the article's Creative Commons licence, unless indicated otherwise in a credit line to the material. If material is not included in the article's Creative Commons licence and your intended use is not permitted by statutory regulation or exceeds the permitted use, you will need to obtain permission directly from the copyright holder. To view a copy of this licence, visit <http://creativecommons.org/licenses/by/4.0/>.

References

- Aghajannezhad, P., Sellier, M., Becker, S.: Patching Hele–Shaw cells to investigate the flow at low Reynolds number in fracture networks. *Transp. Porous Media* **136**, 147–163 (2021). <https://doi.org/10.1007/s11242-020-01505-x>
- Al-Sumaily, D.F., Sheridan, J., Thompson, M.C.: Analysis of forced convection heat transfer from a circular cylinder embedded in a porous medium. *Int. J. Therm. Sci.* **51**, 121–131 (2012). <https://doi.org/10.1016/J.IJTHEMALSCI.2011.08.018>
- ASHRAE Handbook (American Society of Heating and Air-Conditioning Engineers) (2021). https://www.techstreet.com/ashrae/ashrae_handbook.html
- Bear, J.: *Hydraulics of Groundwater*. McGraw-Hill, New York (1979)
- Bejan, A., Kraus, A.D.: *Heat Transfer Handbook*. Wiley, Hoboken (2003)
- Carslaw, H.S., Jaeger, J.C.: *Conduction of Heat in Solids*, 2nd edn. Oxford University Press, New York (1946)
- Casasso, A., Sethi, R.: Efficiency of closed loop geothermal heat pumps: a sensitivity analysis. *Renew. Energy* **62**, 737–746 (2014). <https://doi.org/10.1016/j.renene.2013.08.019>

- Cheng, P.: Heat transfer in geothermal systems. *Adv. Heat Transf.* **14**, 1–105 (1978). [https://doi.org/10.1016/S0065-2717\(08\)70085-6](https://doi.org/10.1016/S0065-2717(08)70085-6)
- Cheng, P.: Mixed convection about a horizontal cylinder and a sphere in a fluid saturated porous medium. *Int. J. Heat Mass Transf.* **25**, 1245–1247 (1982). [https://doi.org/10.1016/0017-9310\(82\)90219-8](https://doi.org/10.1016/0017-9310(82)90219-8)
- Cheng, P., Minkowycz, W.J.: Free convection about a vertical flat plate embedded in a porous medium with application to heat transfer from a dike. *J. Geophys. Res.* **82**, 2040–2044 (1977). <https://doi.org/10.1029/JB082i014p02040>
- Di Pippo, R.: *Geothermal Energy as a Source of Electricity—A Worldwide Survey of the Design and Operation of Geothermal Power Plants*. U.S. Department of Energy, Washington (1980)
- Di Pippo, R.: *Geothermal Power Plants—Principles, Applications, Case Studies and Environmental Impact*, 4th edn. Elsevier, Amsterdam (2015)
- Diao, N., Li, Q., Fang, Z.: Heat transfer in ground heat exchangers with groundwater advection. *Int. J. Therm. Sci.* **43**(12), 1203–1211 (2004). <https://doi.org/10.1016/j.ijthermalsci.2004.04.009>
- Eckert, E.R.G., Drake, R.M.: *Analysis of Heat Mass Transfer*. McGraw-Hill, New York (1972)
- Garg, S.K., Kassoy, D.R.: Convective heat and mass transfer in hydro-thermal systems. In: Rybach, L., Muffler, L.J.P. (eds.) *Geothermal Systems*, pp. 37–76. Wiley, New York (1981)
- Hillel, D.: *Introduction to Soil Physics*. Academic Press, San Diego (1982)
- Holmberg, H., Acuña, J., Næss, E., Sønju, O.K.: Thermal evaluation of coaxial deep borehole heat exchangers. *Renew. Energy* **97**, 65–76 (2016). <https://doi.org/10.1016/j.renene.2016.05.048>
- Katsura, T., Nagano, K., Takeda, S., Shimakura, K.: Heat transfer experiment in the ground with ground water advection. In: *Proceedings of 10th the Energy Conservation Thermal Energy Storage Conf. Ecostock*, pp. 1–7 (2006). <https://citeseerx.ist.psu.edu/viewdoc/summary?doi=10.1.1.516.9933>
- Kimura, S.: Forced convection heat transfer about an elliptic cylinder in a saturated porous medium. *Int. J. Heat Mass Transf.* **31**, 197–199 (1988a). [https://doi.org/10.1016/0017-9310\(88\)90236-0](https://doi.org/10.1016/0017-9310(88)90236-0)
- Kimura, S.: Transient force convection heat transfer from a circular cylinder in a saturated porous medium. *Int. J. Heat Mass Transf.* **32**, 192–195 (1989). [https://doi.org/10.1016/0017-9310\(89\)90103-8](https://doi.org/10.1016/0017-9310(89)90103-8)
- Kimura, S.: Chap. 24 groundwater flows and velocity measurements. In: Vafai, K. (ed.) *Handbook of Porous Media*, 3rd edn., pp. 841–868. CRC Press, Boca Raton (2015)
- Kimura, S.: Transient heat transfer from a circular cylinder with constant heat flux in a saturated porous layer; application to underground water velocimetry. In: *International Symposium on Geothermal Energy*, Kumamoto and Beppu, Japan, Nov. 10–14 (1988b). <https://www.geothermal-energy.org/pdf/IGAstandard/Japan/1988/Kimura.pdf>
- Layeghi, M., Nouri-Borujerdi, A.: Fluid flow and heat transfer around circular cylinders in the presence and no-presence of porous media. *J. Porous Media* **7**(3), 239–247 (2004). <https://doi.org/10.1615/JPorMedia.v7.i3.70>
- Lee, C., Lam, H.: Effects of groundwater flow direction on performance of ground heat exchanger borefield in geothermal heat pump systems using 3-d finite difference method. In: *Proceedings of building simulation*, pp. 337–341 (2007). <https://www.aivc.org/resource/effects-ground-water-flow-direction-performance-ground-heat-exchanger-borefield-geothermal>
- Li, B., Han, Z., Hu, H., Bai, C.: Study on the effect of groundwater flow on the identification of thermal properties of soils. *Renew. Energy* **147**, 2688–2695 (2020). <https://doi.org/10.1016/j.renene.2018.06.108>
- McKibbin, R., Kimura, S.: Heat flow from a buried cylindrical tank partially submerged in groundwater. In: *Proceedings of the 5th International Conference on Porous Media and Its Applications in Science and Engineering*, June 22–27, Kona, Hawaii (2014). http://dc.engconfintl.org/porous_media_V
- Merkin, J.H.: Free convection boundary layers on axi-symmetric and two-dimensional bodies of arbitrary shape in a saturated porous medium. *Int. J. Heat Mass Transf.* **22**, 1461–1462 (1979)
- Nasr, K., Ramadhani, S., Viskanta, R.: An experimental investigation on force convection heat transfer from a cylinder embedded in a packed bed. *ASME J. Heat Transf.* **116**, 73–78 (1994). <https://doi.org/10.1115/1.2910886>
- Ngo, C.C., Lai, F.C.: Heat transfer analysis of soil heating systems. *Int. J. Heat Mass Transf.* **52**, 6021–6027 (2009). <https://doi.org/10.1016/j.ijheatmasstransfer.2009.07.011>
- Nield, D.A., Bejan, A.: *Convection in Porous Media*. Springer, Berlin (2013). <https://doi.org/10.1007/978-1-4614-5541-7>
- Rees, D.A.S., Bassom, A.P., Pop, I.: Forced convection past a heated cylinder in a porous medium using a thermal non-equilibrium model: boundary layer analysis. *Eur. J. Mech.* **B22**, 473–486 (2003)
- Rosli, M.I., Pourkashanian, M., Ingham, D.B., Ma, L., Borman, D., Ismail, M.S.: Transparent PEM fuel cells for direct visualization experiments. In: *ASME 2009 7th International Conference on Fuel*

- Cell Science, Engineering and Technology, June 8–10, 2009, Newport Beach, California, USA. <https://doi.org/10.1115/1.4001353>
- Sarbu, I., Sebarchievici, C.: Solar heating and cooling: Fundamentals, experiments and applications. Elsevier: Oxford, UK (2016).
- Schubert, G., Straus, J.M.: Two-phase convection in a porous media. *J. Geophys. Res.* **82**, 3411–3421 (1977). <https://doi.org/10.1029/JB082i023p03411>
- Schubert, G., Straus, J.M.: Steam-water counterflow in porous media. *J. Geophys. Res.* **84**, 1621–1628 (1979). <https://doi.org/10.1029/JB084iB04p01621>
- Thevenin, J., Sadaoui, D.: About enhancement of heat transfer over a circular cylinder embedded in a porous medium. *Int. J. Heat Mass Transf.* **22**, 295–304 (1995). [https://doi.org/10.1016/0735-1933\(95\)00014-3](https://doi.org/10.1016/0735-1933(95)00014-3)
- Vafai, K.: *Handbook of Porous Media*, 3rd edn. CRC Press, Boca Raton (2015)
- Valavanides, M.S.: Review of steady-state two-phase flow in porous media: Independent variables, universal energy efficiency map, critical flow conditions, effective characterization of flow and pore network. *Transp. Porous Media* **123**(1), 45–99 (2018). <https://doi.org/10.1007/s11242-018-1026-1>
- Wang, H., Qi, C., Du, H., Gu, J.: Thermal performance of borehole heat exchanger under groundwater flow: a case study from Baoding. *Energy Build.* **41**(12), 1368–1373 (2009). <https://doi.org/10.1016/j.enbuild.2009.08.001>
- Wong, W.S., Rees, D.A.S., Pop, I.: Forced convection past a heated cylinder in a porous medium using a thermal non-equilibrium model: finite Péclet number effects. *Int. J. Therm. Sci.* **43**(3), 213–220 (2004). <https://doi.org/10.1016/j.ijthermalsci.2003.07.005>
- Zimmerman, R.W., Bodvarsson, G.S.: Hydraulic conductivity of rock fractures. *Transp. Porous Media* **23**, 1–30 (1996). <https://doi.org/10.1007/BF00145263>

Publisher's Note Springer Nature remains neutral with regard to jurisdictional claims in published maps and institutional affiliations.